Journal Name

Cite this: DOI: 10.1039/xxxxxxxxxx

Aggregation enhancement of coronene molecules by seeding with alkali-metal ions†

M. Bartolomei,[a] F. Pirani,[b] J. M. C. Marques*[c]

Received Date
Accepted Date

DOI: 10.1039/xxxxxxxxxx

www.rsc.org/journalname

Microsolvation constitutes the first step in the formation of cluster structures of molecules that surround the solute in the bulk and it allows for a deep insight about the relationship between the structure of the solvation shells and other physical properties. We propose semiempirical potential energy functions that are able to describe the interaction between K^+ or Cs^+ with coronene. Such functions were calibrated through the comparison with accurate estimations of the interaction between the cation and the planar hydrocarbon, obtained by means of *ab initio* electronic-structure calculations. By employing the potential energy functions and an evolutionary algorithm (EA), we have investigated the structure and energetics of the clusters resulting from the microsolvation of either K^+ or Cs^+ with coronene molecules. The reliability of the results for smaller clusters were checked by performing geometry re-optimization exploiting a suitable DFT level of theory. This has allowed for the characterization of the first solvation shells of large and planar molecules of coronene around an alkali-metal ion. It has been also found that the presence of metal ion impurities considerably enhances the formation of small coronene clusters leading to much stronger binding energies for heterogeneous with respect to homogeneous aggregates. These clusters could represent relevant species involved in the early stages of soot nucleation.

1 Introduction

Coronene is a polycyclic aromatic hydrocarbon (PAH) molecule usually employed as a benchmark system to study physical processes involving π-π interactions, since it is formed by seven fused benzene-type rings. As similar or smaller size PAHs, coronene has been identified in the interstellar medium [1,2] and it is present in the earth atmosphere as a pollutant species mostly deriving from combustion processes [3,4].

This PAH molecule is also the smallest prototype of a graphene layer and, hence, it is usually used by theoreticians to investigate adsorption phenomena. This type of carbon materials has shown good electrochemical performance when used as anodes in rechargeable batteries, since the adsorption of alkali metals on the 2D surface is reversible [5,6]. Such adsorption leads to the formation of structures with alkali-metal ions in between the graphene layers of the graphite anode. This process as well as the corresponding structural properties of the adducts of polyaromatic anions with alkali metal counterions have been reviewed [7]. Another recent review [8] describes the role of coronene for the great enhancement of the solubility of C_{60} due to the formation of a pseudosolvent nano phase based on supramolecular coordination structures [9].

Recently, we have exploited a new potential energy surface (PES) for coronene clusters (henceforward designated as Cor_n) given in an analytical form and whose parameters have been fine tuned on results from high level electronic structure methods. Such PES has been exploited to search for low-energy structures, which allowed us to identify columnar-like configurations and a variety of multistack arrangements as the most stable motifs in the small- and large-size range of clusters, respectively [10]. While we have found pure columnar structures for the most stable configurations only up to $n = 5$, other global optimization studies [11,12], which were based on less realistic force-field models for Cor_n, have reported single-stack global minima for clusters up to $n = 7$. The proposed PES was expected to be reliable also for large clusters, as confirmed by its capability to reproduce some of the features of the most stable β -herringbone polymorph of coronene [10].

By extending the methodology previously applied for Cor_n [10], in this work we want to investigate the structure of the corre-

[a] *Instituto de Física Fundamental, Consejo Superior de Investigaciones Científicas (IFF-CSIC), Serrano 123, 28006 Madrid, Spain.*
E-mail: maxbart@iff.csic.es
[b] *Dipartimento di Chimica, Biologia e Biotecnologie, Università di Perugia, 06123 Perugia, Italy.*
E-mail: pirani.fernando@gmail.com
[c] *CQC, Department of Chemistry, University of Coimbra, 3004-535 Coimbra, Portugal.*
E-mail: qtmarque@ci.uc.pt

† Electronic Supplementary Information (ESI) available: [details of any supplementary information available should be included here]. See DOI: 10.1039/b000000x/

sponding microsolvation clusters of potassium and cesium ions, *i.e.*, K^+Cor_n and Cs^+Cor_n, with particular emphasis on the first solvation shells. We should mention that microsolvation is a stepwise process where a number of solvent molecules are added in the surroundings of a given species (*i.e.*, the solute) to form aggregates of increasing size and, hence, it should not be necessarily associated to a specific state of matter (*e.g.*, the liquid state). As the microsolvation cluster grows up, it becomes possible to study the structure and other properties of the solvation shells at the molecular level. In particular, the structural features of the most stable clusters may be well characterized by applying state-of-the-art global optimization techniques. Accordingly, the basin-hopping approach [13] and methods based on genetic algorithms [14–16] are perhaps among the most applied to discover low-energy structures of microsolvation clusters. In our group, we have used our own evolutionary algorithm [16] (EA) to perform microsolvation studies involving several ions and solvent molecules [17].

One of the goals of this investigation is to find out how the global minimum structures as well as other low-energy motifs of Cor_n aggregates vary in presence of metal ion impurities. Indeed, the role of the metal ion as a seeding species capable to facilitate and improve the aggregation of Cor_n clusters is of high relevance for the atmosphere modeling. In fact, trace metals could be present in flames and those clusters can represent intermediate complexes involved in the soot nucleation [18], a process not fully understood yet [19,20].

The effect of the size of the aromatic-type molecules surrounding the ion may be assessed by comparing the present study against previous global optimization results on the microsolvation of K^+ and Cs^+ with benzene [21]. Moreover, the binding for heavier alkaline ion Cs^+-Cor and Cor-Cor dimers is expected to fall in the same energy scale. However, other different features of the related PESs, arising from the critical balance of interaction components involved, which have different nature, strength and radial dependence, can emphasize relevant selectivity in the cluster formation.

The methodology followed in this work is detailed in Section 2, where we describe the interaction-potential model proposed for the K^+-Cor_n and Cs^+-Cor_n clusters, as well as the electronic-structure calculations that we have employed to improve the parametrization of the PES. Also in Section 2, we give the main ingredients of the EA used in the global optimization of clusters. In Section 3, we present and discuss the results of this microsolvation study, including the features of the coronene-cation potential. Finally, a summary of the main achievements are given in Section 4.

2 Methodology

2.1 Electronic-structure calculations

In order to obtain reference *ab initio* values for the coronene-cation interaction energy the use of the coupled-cluster with single, double and perturbative triple excitations (CCSD(T)) approach together with extended basis sets would be highly desirable. However, the large size of the considered PAH does not allow such an option and therefore we have chosen to rely on more computationally affordable post-Hartree Fock methods, such as second-order Møller-Plesset perturbation theory (MP2) and its spin-component scaled modification (MP2-SCS) [22].

The reliability of the latter approaches for an analogous and prototypical system of reduced size, such as benzene-K^+, has been first tested and related interaction profiles for different limiting configuration of the complex are depicted in Fig. 1, together with reference CCSD(T) energies. All reported results correspond to the aug-cc-pVTZ [23] and def2-ATZVPP [24] basis sets, for benzene and K^+, respectively. It can be appreciated that the MP2-based results well reproduce the benchmark CCSD(T) values for both perpendicular and in-plane approaches of the ion with respect to the molecular plane. More in details, a slightly better agreement can be appreciated in the case of the MP2-SCS profile for the "hollow" configuration. We believe that this comparison validates the chosen MP2 approaches for the determination of accurate interaction energies within benzene-cation systems and also promotes their use for the study of aggregates containing larger aromatic species such as coronene. The coronene-cation (K^+,Cs^+) interaction energies obtained at the MP2 and MP2-SCS levels for four different limiting configurations of the complex are reported in Fig. 2 and they correspond to the aug-cc-pVTZ [23] and def2-AQZVPP [24] basis sets, for coronene and cation (K^+,Cs^+), respectively. We have checked that the chosen (aug-cc-pVTZ/def2-AQZVPP) basis sets provide well converged interaction energies: differences with respect to the reduced aug-cc-pVTZ/def2-ATZVPP sets are within 3% around the minima.

In order to make MP2-based calculations tractable, the density-fitting method [25] has been applied to approximate the two-electron repulsion integrals. All reported interaction energies are defined as the energy difference between the complex and infinitely separated monomers, treated as rigid bodies and having the same geometry as in the aggregate. Moreover, the counterpoise method [26] was applied to correct for the basis set superposition error (BSSE). All MP2 computations have been performed by using the MOLPRO2012.1 package [27].

To perform the re-optimization of some specific minimum configurations predicted by the EA for the K^+-Cor_n clusters (see Section 3) it is necessary to turn to DFT level of theory since related MP2 computations would not be feasible. In particular, the generalized gradient approximation of Perdew, Burke, and Ernzerhof (PBE) [28] has been employed together with the dispersion contribution corrections as implemented in the DFT-D3(BJ) method of Grimme [29] as well as the cc-pVTZ basis set [23]. We have tested the PBE-D3(BJ) interaction energies for K^+-coronene against the corresponding MP2 and MP2-SCS values. These data, properly corrected for the BSSE, are presented for four K^+-coronene approaches in Figure S1 of the Supplementary Information where we may observe that the PBE-D3(BJ) interaction energies are consistent with those obtained at the MP2 and MP2-SCS levels, especially in the minimum region of the most attractive configurations.

All DFT calculations were carried out with the GAUSSIAN 09 package [30].

2.2 Analytical potential model

In the present study, the coronene (Cor) molecules have been assumed to be a rigid body, in which the C_0-C bond lengths and C-C-C angles were set to 1.420 Å and 120 , respectively, whereas C-H bond lengths and C-C-H angles were chosen to be 1.090 Å and 120°, respectively.

For clusters formed by one cation and n Cor monomers, the total interaction potential is here defined as the sum of two contributions, namely the Cor – ion and Cor – Cor components. The Cor – Cor interaction has been described as detailed in Ref. 10, where the related analytical potential is presented. The Cor – ion component of the interaction potential has been instead formulated as follows:

$$V = \sum_{k=1}^{n} V_{el,k} + V_{nel,k} \qquad (1)$$

where the first and second terms refer to the electrostatic and non-electrostatic contributions, respectively. The calculation of $V_{el,k}$ assumes for Cor the same charge distribution introduced in Ref. 10 consisting of 48 and 12 point charges associated to the C and H atoms, respectively. The electrostatic potential energy for each Cor-ion pair is then calculated as sum of Coulomb contributions by following the expression:

$$V_{el} = \sum_{i=1}^{48} \frac{q_{ion} q_C}{4\pi\varepsilon_0 r_{ion-C_i}} + \sum_{i=1}^{12} \frac{q_{ion} q_H}{4\pi\varepsilon_0 r_{ion-H_i}} \qquad (2)$$

where r_{ion-C_i} and r_{ion-H_i} are the distances between the cation and the point charges related to the C and H atoms of the k^{th} Cor molecule, respectively.

As for the Cor – ion non-electrostatic energy, as usually it is described as a sum of atomic ion-"effective atom" contributions involving interaction pair-potentials between the ion and the atoms on the Cor molecule, *i.e.*,

$$V_{nel} = \sum_{i=1}^{24} V_{ion-C_i} + \sum_{i=1}^{12} V_{ion-H_i} \qquad (3)$$

The last expression exploits the combination of "effective" contributions, in the sense that each pair potential depends on the behavior of the ion and of any effective atom within the Cor molecule.

The adopted effective atomic electronic polarizability is different from that of the isolated atom since takes into account of its participation in stable chemical bonds. Moreover, the sum of all effective atomic values must be consistent with the polarizability of the Cor molecule. In equation 3, each term is described by an improved Lennard-Jones (ILJ) potential function V_{ILJ} [31–33], which depends on the separation distance, r, between the two interacting centers according to the expression:

$$V_{ILJ} = \varepsilon \left\{ \frac{m}{n(r)-m} \left(\frac{r_0}{r}\right)^{n(r)} - \frac{n(r)}{n(r)-m} \left(\frac{r_0}{r}\right)^{m} \right\} \qquad (4)$$

where ε and r_0 are, respectively, well depth and equilibrium distance associated to each specific ion-"effective atom" pair potential. The m parameter is here chosen equal to 4 as usual for ion-neutral systems. The $n(r)$ exponent, defining simultaneously the falloff of the atom-atom repulsion and the strength of the attraction, is expressed as

$$n(r) = \beta + 4.0 \left(\frac{r}{r_0}\right)^2 \qquad (5)$$

The first term in Eq. (4) describes the size (or Pauli) repulsion, while the second one represents the induction attraction including also dispersion contributions.

Due to the additional β parameter and to the proper $n(r)$ dependence, the ILJ function becomes more flexible and more realistic than the classical LJ model, removing most of its inadequacies due to an excessive attraction and to a too strong repulsion. The modulation within limiting ranges of β allows also to indirectly include additional interaction components emerging at short range, as perturbative-stabilizing charge transfer effects.

Moreover, the well depth (ε) and equilibrium distance (r_0) parameters, directly associated to charge and polarizability of involved partners [32,34,35], assume a transferable character since the effective C and H atomic polarizabilities are nearly independent for aromatic species of different kind.

As zero order parameters for the non-electrostatic ion-atom contributions we considered those reported in Ref. 17 and related to the cation-benzene interaction. However, an optimization of some of them was needed in order to obtain a better agreement with the electronic structure interaction energy results, obtained as described in the previous subsection. In any case, the variations of the parameters, defining V_{nel}, have been kept within limited ranges in order to maintain a proper physical meaning and do not become simple fitting variables. Specifically, the highest allowed variation with respect to the zero order values has been of 20% and 4% for ε and r_0, respectively. These adjustments have been sufficient to obtain a good agreement with the *AB initio* estimations within few percents both around the minimum of the interaction potential and in the attractive region at long range. Note also that the interaction component arises from the balance of size repulsion with ion-induced dipole and dispersion attractions, whose individual pair contributions are expected to be similar for cation-benzene and cation-coronene systems. Therefore, fine adjustments of involved parameters can be due to the slightly different conditions of C and H atoms in benzene and coronene molecules. On the other hand, it must be stressed that the value of the q_{ion} charge, appearing directly in the formulation of V_{el} (the leading component that controls the long range behavior of ion-Cor PESs) has been reduced down to 0.6 a.u. to provide, as stressed before, an optimal accord with the electronic structure calculations. This reduction has been necessary since we have chosen to maintain the same charge distribution on coronene monomers introduced in Ref. 10 in order to directly use the PES in there proposed. We have checked by means of DFT population analysis calculations that around the global minimum configuration of the K^+-Cor dimer the ion charge assumes, indeed, a reduced value which is well consistent with that here considered. The charge redistribution within the interacting adducts probably arises from charge transfer effects, which, in the adopted parametrization, are indirectly enclosed by the modulation of the

two selected components.

All final parameters used for the atom-atom interactions are reported in Table 1.

2.3 Geometry optimization

The low-energy structures of the K^+Cor_n and Cs^+Cor_n clusters were searched by employing the hybrid evolutionary algorithm (EA) developed in our group [16]. This method combines a global optimization strategy with a local search to reach the minimum structure at the bottom of each basin of attraction; the local optimization uses the limited memory Broyden-Fletcher-Goldfarb-Shanno (L-BFGS) algorithm [36,37], which is a very efficient quasi-Newton method. Although the applications of our EA for discovering the global minima of molecular clusters have been recently reviewed [17], we should especially emphasize that it has been adequate to study the microsolvation of alkali-metal ions with different solvent molecules [21,38,39]. In the remaining of this section, we just describe the main ingredients of the EA and the reader is addressed to Refs. 16,17 for details.

The EA follows a generational approach for the evolution of the pool of structures that constitute possible solutions for the global optimization problem. The algorithm treats the monomers of the cluster (*i.e.*, the coronene molecules) as rigid bodies that can be defined by the corresponding center-of-mass positions and the orientation Euler-angles. Thus, a solution in the pool is formed by n six-tuples (n stems for the number of coronene molecules), each one encoding the Cartesian coordinates of the center-of-mass and the Euler angles of the corresponding monomer.

The initial population of solutions forming the pool is randomly generated and, subsequently, local optimized with the L-BFGS algorithm. Then, it evolves to the next generation by applying genetic operators that alter the solutions. Our approach rely on the simulated binary crossover [40] to combine pairs of promising solutions that were selected through tournament; this involves the choice of the best among five solutions that were randomly selected from the pool. Within a given probability, the structures so obtained are, afterward, slightly modified by applying sigma mutation [41] both to the center-of-mass positions and orientation angles of a few coronene molecules of the microsolvation cluster. Lastly, all new structures are optimized by applying the L-BFGS algorithm [36,37]. The EA always replaces the old population by the new offspring solutions, but it applies an elite operator to avoid lost the lowest-energy structure from the present generation to the following one. Such iterative procedure (usually designated as a run) is conducted until 10000 evaluations of the potential energy function are reached; in addition, a limited number of runs with 30000 evaluations were also performed for clusters with more than ten coronene molecules. Since this is a stochastic method, the EA was run, at least, 10 times to guarantee statistically meaningful results. The putative global minimum structure is the lowest-energy solution achieved after all runs are completed for a given cluster size. The EA also saves a given number of other low-energy structures besides the global minimum, which are relevant for the subsequent analysis. We further note that, unless mentioned, the values of the EA settings are the same as in our previous work on benzene [42].

3 Results and discussion

3.1 Coronene-cation dimer

The main features of the interaction for the coronene-K^+ and coronene-Cs^+ dimers arranged in four different limiting geometries are shown in Figure 2. These configurations are referred to as "hollow", "top", "in-plane 1" and "in-plane 2". In the first two the ion is perpendicularly approaching the coronene molecule towards the geometric center and on top of the inner ring C atom, respectively. The last two correspond instead to in-plane approaches along the x_1 and x_2 coordinates which point to the C-C and C-H bonds of coronene, respectively, as displayed in Figure 2.

First of all, it can be observed that the perpendicular approaches are by far those leading to the most attractive interaction energies, as it could be expected by considering the dominant electrostatic interaction between the cation and the negative charges distributed on the carbon plane.

Moreover, it can be also appreciated that the well depth of coronene-K^+ electronic structure interaction is globally more attractive than that of coronene-Cs^+, with the corresponding minimum positions of the lighter dimer shifted at lower values of the intermolecular coordinate. However, in all cases a larger attraction can be also appreciated for coronene-Cs^+ in the long range component. These trends can be rationalized by taking into account that the larger size and consequently the larger polarizability of the Cs^+. The latter provides an increased dispersion attractive contribution in the long range, which sums up to the dominant attractive electrostatic component, but also determines a larger orbital overlap and therefore repulsion in the intermediate and short intemolecular distance ranges.

Figure 2 also reports the optimized PES predictions as solid lines: a good agreement in what concerns the size and position of the first-principles energy results (depicted as squares and circles) as well as their relative stability order can be observed. In particular, the model PES results are well in between the MP2-SCS (full symbols) and MP2 (shaded symbols) interaction energies in all considered cases. According to the results here obtained, it is also worth to notice that while in the most stable (the equilibrium) configuration the binding energy of the cation-Cor systems is only about 30% larger than that for Cor-Cor dimer (see for instance Fig. 2 of Ref. 10), at large separation distances the asymptotic attraction is completely different in the two cases. In particular, in such distance region the V_{el} interaction component makes the most stable configuration in the ion-Cor dimer at least a factor 2–3 more attractive with respect to that in the Cor-Cor counterpart. These interaction features and the competition between them will be considered crucial in determining the structures of the ion-Cor_n clusters, as seen in the next section.

3.2 Structures

We show in Figures 3 and 4 the global minimum structures of the K^+Cor_n and Cs^+Cor_n ($n = 1 - 15$) microsolvation clusters, respectively. Although not clearly shown in these figures, we should note that the global minimum for $n = 1$ corresponds to a structure

where the ion arises in a "hollow" position (as described in Figure 2), whereas along the "top" approximation to the coronene monomer we have identified, by means of DFT calculations, a second-order saddle-point instead of a local minimum. It is apparent from these figures that, despite the difference of size between K^+ and Cs^+, the coronene molecules tend to be organized in the same manner around the two ions. Exceptions arise for $n = 12$, 13 and 15: K^+Cor_{12} and K^+Cor_{13} (K^+Cor_{15}) show three (six) sets of stacked molecules, while the corresponding Cs^+Cor_n clusters present always five sets of stacks. By comparing the structures in Figures 3 and 4 with the pure coronene clusters (see Figure 3 of Ref. 10), one concludes that the presence of either K^+ or Cs^+ leads to less stacked structures (with less than 3 monomers per stack), especially for $n \leq 8$. Indeed, the columnar-type structures observed for Cor_n ($n \leq 5$) are, now, absent due to an organization of the coronene monomers that favor a maximization of the number of solvent molecules around the ion. It is worth noting that the first structure with more than two monomers in a stack arise only at $n = 9$. Larger clusters show multi-stacked structures with increasing number of monomers per stack, but "handshake" association motifs observed for Cor_n clusters [10,12] are not present in the microsolvation of K^+ and Cs^+ by coronene.

It is particularly interesting to notice that the global minimum structures of the K^+Cor_n and Cs^+Cor_n clusters up to $n = 3$ somehow resemble those previously found [21] for the microsolvation of Na^+, K^+ and Cs^+ with benzene (Bz), where the distribution of the Bz molecules tend to maximize the interactions with the ion. Conversely, stacked-type configurations that are favored for both K^+Cor_n and Cs^+Cor_n with $n \geq 4$ (*cf.* Figures 3 and 4) cannot be found as global minima of the Na^+Bz_n, K^+Bz_n and Cs^+Bz_n clusters [21]. This can be attributed to a quite stronger ion-benzene interaction (see Figure 1) with respect to that for the benzene dimer (see Fig. 1 of Ref. 10).

In Figure 5, we represent the distances between the ion and the center of each coronene molecule as a function of the cluster size. Despite the expected tendency for showing larger values of the Cs^+-Cor distances, the scatter plots for K^+Cor_n and Cs^+Cor_n are very similar, which is compatible with the aforementioned considerations about the global minimum structures. We may observe in Figure 5 that the closure of the first solvation shell occurs at $n = 3$ for both K^+ and Cs^+, whereas a maximum of four monomers can be accommodated close to the microsolvated ions when the solvent is the smaller benzene molecule [21]. For the latter, the above mentioned stronger ion-benzene interaction in comparison to the benzene-benzene one is expected to favor a larger number of monomers around the ion than in the case of coronene.

In turn, larger ion-coronene distances arise for $n \geq 4$, which can be associated to the formation of stacks that grow with the addition of more molecules to the cluster. Accordingly, pronounced jumps occur in the points of Figure 5 for $n = 4$, 9, and 11, which correspond to the addition, respectively, of the second, third, and fourth molecule to one of the stacks. Cluster sizes in between are associated to plateaus of the larger ion-coronene distances, which is due to the addition of molecules to the shorter stacks until they reach the same length. In the case of the ion-benzene$_n$ clusters [21], we also observe jumps in the corresponding scatter plots at $n = 5$ and 13, which leads to a clear definition of only three solvation shells for K^+Bz_n and Cs^+Bz_n.

Besides the global-minimum structures, it is also important to look at other structural motifs. Some of the most representative are shown in Figure 6 and Figure 7 for K^+Cor_n and Cs^+Cor_n (with $n = 2 - 6$), respectively. We mainly focus on columnar-, herringbone- and cage-type structures; although not shown, several variants of the three types of structure and, also, of the corresponding global minimum motif can be found. We may observe in these figures many columnar motifs, most of which form a sandwich-type structure with the ion in between two coronene molecules, while other show a stack with monomers disposed asymmetrically and the ion placed in the equatorial position of the middle one; for some columnar structures, there is at least one coronene molecule that arises in a position almost perpendicular to the main stack. Conversely, herringbone- and cage-type structures are not so frequent and, even, they do not appear for some cluster sizes. Indeed, both motifs cannot be observed for $n = 2$ and 3, while for $n = 4$ a herringbone-type structure with 28.8 kJmol^{-1} above the global minimum appears in the case of Cs^+ (but not for K^+). In general, herringbone- and cage-type structures are among the motifs with lower energy; the only exception occurs for the cage-type structure of K^+Cor_4, whose energy is 54.5 kJmol^{-1} above the global minimum. In contrast, among columnar-type structures one can find both low and high energy motifs, which is related to the number of monomers forming the longest stack, *i.e.*, longer stacks are less stable.

We notice in Figure 6 and Figure 7 that, in general, the low-energy structures are similar for the K^+Cor_n and Cs^+Cor_n (with $n = 2 - 6$) clusters. Nonetheless some subtle differences arise between the related structures. In particular, the low-lying structures of K^+Cor_2 (K^+Cor_3) show higher (lower) energies than Cs^+Cor_2 (Cs^+Cor_3). It is also interesting to note that the structure of K^+Cor_3 with 12.0 kJmol^{-1} does not appear for Cs^+Cor_3. Additionally, energy reorder can be observed for some structures at $n = 4$ and 5. Finally, it is important to mention that structures similar to the present stacked- and cage-type motifs have been recently reported [43] in a molecular dynamics simulation of coronene in the presence of K^+ at 500 K .

3.3 Energetics

The stability of growing microsolvation clusters may be inferred from the average binding energy:

$$E_n = -\frac{E_{GM,n}}{n} \tag{6}$$

where $E_{GM,n}$ designates the energy of the putative global minimum for each cluster size, n. We should note that the binding energy may be separated into two contributions: ion-coronene and coronene-coronene interactions. In the top panel of Figure 8, we represent the binding energies of the K^+Cor_n and Cs^+Cor_n clusters, as well as the corresponding contributions due to ion-coronene and coronene-coronene interactions. Figure 8(a) shows that E_n has a similar behavior for both systems: in the microsolva-

tion of K^+ (Cs^+), the binding energy increases up to $n = 2$ ($n = 3$) and, then, decreases for larger clusters. Such behavior is corroborated by DFT calculations for K^+Cor_n ($n = 1-5$), as shown by the black asterisks in Figure 8. The major differences between the binding energies of the K^+Cor_n and Cs^+Cor_n clusters occur for the smaller clusters (for $n < 3$), which may be attributed to the ion-coronene component of the interaction (see also Figure 2). Indeed, this component tends to decrease with the increasing size of the clusters. Conversely, the coronene-coronene component of the energy increases with the cluster size, as already seen in the case of pure Cor_n clusters (see Fig. 4 of Ref. 10), and it crosses the ion-coronene curve at about $n = 6$. It is important to emphasize that the different stability of the smaller adducts catalyzes the competition that follows in the formation of larger clusters.

The second energy difference, *i.e.*,

$$\Delta_2 E = E_{GM,n-1} - 2E_{GM,n} + E_{GM,n+1} \quad (7)$$

is another relevant parameter to discuss the relative stability of the microsolvation clusters. In Eq. (7), $E_{GM,n-1}$, $E_{GM,n}$ and $E_{GM,n+1}$ are the global minimum energies at the sizes $n-1$, n and $n+1$, respectively. We emphasize that the so-called "magic numbers" correspond to particularly stable structures in comparison to their neighbor sizes and are assigned to the maxima of the $\Delta_2 E$ function. It is interesting to observe in Figure 8(b) that the second energy difference shows subtle differences between K^+Cor_n and Cs^+Cor_n, which may be attributed to the relative sizes of the two ions and the difficulty to accommodate large coronene molecules in the first solvation shell. In fact, as one may observe in Figure 5, the distances between the ion and the nearest-neighbor coronene molecules are, in general, closer to the corresponding equilibrium geometry in the case of Cs^+ than for K^+, which then favors the Cs^+-coronene energy contribution. Thus, whereas four peaks appear for the Cs^+ microsolvation clusters, only two are prominent for K^+Cor_n clusters. However, the most relevant magic numbers arise for K^+Cor_2 and Cs^+Cor_3, which also correspond to maxima of the binding energy and are somehow related to the filling the first solvation shell. Although not so prominent, the "magic number" arising for the K^+Cor_2 cluster is confirmed by DFT calculations (*cf.* black asterisks in Figure 8(b)).

From the comparison of present results with those related to the pure Cor_n clusters (see Ref. 10) important differences can be emphasized. As expected, these differences are mainly apparent for smaller clusters, since the ion-coronene interaction is the major contribution at $n \leq 6$ (see above). Thus, the K^+Cor_n and Cs^+Cor_n global minimum structures show the ion species surrounded by the coronene molecules, leading to various stacks as the cluster is growing up, whereas the lowest-energy minima of Cor_n (with $n \leq 5$) are formed by only one stack [10]. Such growing pattern achieved in the presence of the ion leads to more spherical shapes. Another important feature due to the presence of an alkali-metal ion is the enhancement of the average binding energy, which, as stressed above, is particularly evident in the case of the smaller clusters ($n < 6$) for which present values are at least a factor 2 higher than for Cor_n. Present total binding energies obtained for the K^+Cor_n clusters up to $n = 5$ are reported in Table 2, which correspond to the global minima structures from the analytical potential and to those reoptimized at the DFT level (see Section 2.1). The DFT binding energy values for $n = 1-3$ suggest that non-additive many body effects, not explicitly taken into account in the analytical potential, are around 2-4% and therefore seem to play a negligible role. These findings probably originate from the appreciable value of the ion size that forces the coronene molecules to be confined at sufficiently large separation distances.

Moreover, they are significantly larger than the corresponding ones reported in Table 2 of Ref. 10. Therefore, it can be concluded that the presence of alkali-ion impurities facilitates the formation of particularly stable small coronene clusters, which could represent relevant intermediate species involved in soot nucleation. In fact, molecular dynamics studies [19,44] have shown that incipient soot particles can be formed by nucleation of PAHs at low temperatures (*e.g.*, $T = 400$ K), but such process is dominated by relatively weak interactions and, hence, it becomes more difficult to occur at typical flame temperatures (*i.e.*, $T > 1000$ K). For instance, the formation of coronene clusters with up to 5 monomers (mainly leading to stacked structures), which then can grow to originate incipient soot particles, is expected in simulations [19] at $T = 800$ K, while those small clusters are not stable enough at higher temperatures to proceed the physical nucleation process [19,45]. In turn, the presence of trace iron atoms enhances dramatically the PAH growth and soot nucleation at temperatures above 1500 K, because Fe helps to connect PAHs through the formation of strong chemical bonds after dehydrogenation [18].

4 Conclusions

The characterization of nature and strength of non covalent interaction components, of their role in determining structural and dynamical properties of matter, are of general interest under several fundamental and applied points of view. Specifically, those determining structure and binding energy in ion-Cor_n and Cor_n clusters can be of relevance also for the better understanding of analogous systems involved in the soot formation. New and accurate multidimensional PESs for ion-coronene clusters have been presented. Their formulation is based on an analytical function whose parameters, having a defined physical meanings, have been fine-tuned exploiting accurate electronic structure interaction energy calculations. The adopted methodology is the same used recently (Ref. 10) for the formulation of the multidimensional PES in Cor_n clusters, and this represents a crucial condition to emphasize the competition between the intermolecular interactions in ion-Cor and Cor-Cor pairs, involved in the formation of specific structures in heterogeneous and homogeneous clusters. In particular, the Cor-Cor pair interaction, both at equilibrium and large separation distances, is mostly affected by the V_{nel} component (size repulsion plus dispersion attraction), while V_{el} assumes only a perturbation role. On the other hand, the interaction in ion-Cor pair depends, around the equilibrium configuration, on the competition of size repulsion with induction and dispersion attraction plus an electrostatic contribution, while at large distances it is dominated by the electrostatic term. Since above mentioned interaction components scales in a different way with the separation distance and relative orientation of involved partners, their critical balance is

crucial to define differences in the structure and stability of homogeneous and heterogeneous clusters. Moreover, the obtained force fields provide an internally consistent description of the interactions both in the most stable minimum structures and in all other less-stable minimum structures of the systems. Therefore, the PESs have been successfully used to carry out a global optimization study, based on the EA, for the characterization of cluster structures involving a number n of Cor monomers up to n = 15. The structures so characterized in this paper appear to be rather different with respect to those of corresponding Cor_n (see Figures 3-4 and their comparison with Figure 3 of Ref. 10). Globally, it is found that the presence of alkali-ion impurities enhances the formation of small Cor_n clusters which are characterized by strong binding energies. Present results for ion-coronene (an apolar PAH) systems appear to be consistent and complementary to those recently obtained [43] for aggregates involving curved polar PAHs. In particular, in such study it has been demonstrated the relevance of ion-PAH interaction in determining the nucleation behavior and structure of nascent soot particles. Indeed, it has been also experimentally shown [46] that the addition of alkali metals to atmospheric-pressure flames, where they are readily ionized, leads to a grater number of particles which are characterized by a smaller size with respect to the unseeded flames.

Moreover, EA allowed also to express the clusters average binding energy as a combination of ion-Cor and Cor-Cor contributions: it appears that the former is the dominant component up to n=6, while the latter becomes more important for larger n, since here the removing of a coronene molecule involves the outer solvation shells.

Further insight on the competition of interaction components, in determining energy and structure of heterogeneous clusters, could be obtained by the investigation of systems involving negative halogenated ion whose V_{el}, that tends to favor planar geometries in ion-Cor dimer, should affect markedly the packaging of coronene molecules in the solvation shells. Therefore, also this competition can be then relevant to define the dynamics of some basic elementary steps of complex phenomena occurring in flames, for which it has been also recently observed that the addition of metal salts selectively influences the early stages of the soot formation [47].

Finally, present results suggest that the extension of the investigation to systems including the smallest alkali ion (Li^+) could be of great relevance from one side to generalize the interaction formulation, since charge transfer and many body effects are expected to increase their relative role, and from the other side to study ion-Cor_n clusters involving quite stronger ion-molecule interactions.

Acknowledgments

J.M.C.M. acknowledges the support from the Coimbra Chemistry Centre (CQC), which is financed by the Portuguese "Fundação para a Ciência e a Tecnologia" (FCT) through the Project UID/QUI/00313/2019. J.M.C.M. also acknowledges the COST action "Molecules in Motion" (MOLIM, CM1405) for support. M.B. acknowledges financial support by the Spanish "Ministerio de Ciencia e Innovacion" for the FIS2017-84391-C2-2-P grant. F.P. acknowledges the "Dipartimento di Chimica, Biologia e Biotecnologie dell' Università degli Studi di Perugia". We are grateful for the provision of computational time in the supercomputer resources hosted at Laboratório de Computação Avançada, Universidade de Coimbra, and by CESGA (Spain).

References

1 A. Léger and L. d'Hendecourt, *Ann. Phys. Fr.*, 1989, **14**, 181–206.
2 P. Ehrenfreund, B. H. Foing, L. d'Hendecourt, P. Jenniskens and F. X. Desert, *Astron. Astrophys.*, 1995, **299**, 213–221.
3 P. D. Boehm, *Environmental Forensics*, Academic Press, Burlington, 1964, pp. 313 – 337.
4 M. R. Kholghy, A. Veshkini and M. J. Thomson, *Carbon*, 2016, **100**, 508–536.
5 K. E. A. (Editor), S. A. H. (Editor) and R. V. K. (Editor), *High Energy Density Lithium Batteries: Materials, Engineering, Applications*, Wiley-VCH, Weinheim, 2010.
6 W. van Schalkwijk (Editor) and B. S. (Editor), *Advances in Lithium-Ion Batteries*, Kluwer Academic Publishers, New York, 2002.
7 A. V. Zabula and M. A. Petrukhina, *Advances in Organometallic Chemistry*, Academic Press, 2013, vol. 61, pp. 375 – 462.
8 S. Sadjadi, *Organic Nanoreactors*, Academic Press, Boston, 2016, pp. 257 – 303.
9 K. Suzuki, K. Takao, S. Sato and M. Fujita, *Journal of the American Chemical Society*, 2010, **132**, 2544–2545.
10 M. Bartolomei, F. Pirani and J. M. C. Marques, *J. Phys. Chem. C*, 2017, **121**, 14330–14338.
11 M. Rapacioli, F. Calvo, F. Spiegelman, C. Joblin and D. J. Wales, *J. Phys. Chem. A*, 2005, **109**, 2487–2497.
12 J. Hernï¿½ndez-Rojas, F. Calvo and D. J. Wales, *Phys. Chem. Chem. Phys.*, 2016, **18**, 13736–13740.
13 D. J. Wales and M. P. Hodges, *Chem. Phys. Lett.*, 1998, **286**, 65–72.
14 B. Hartke, *J. Phys. Chem.*, 1993, **97**, 9973–9976.
15 R. L. Johnston, *Dalton Trans.*, 2003, 4193–4207.
16 J. L. Llanio-Trujillo, J. M. C. Marques and F. B. Pereira, *J. Phys. Chem. A*, 2011, **115**, 2130–2138.
17 J. M. C. Marques, F. B. Pereira, J. L. Llanio-Trujillo, P. E. Abreu, M. Albertï¿½, A. Aguilar, F. Pirani and M. Bartolomei, *Phil. Trans. R. Soc. A*, 2017, **375**, 20160198.
18 Q. Mao and K. H. Luo, *Proc. Combust. Inst.*, 2019, **37**, 1023–1030.
19 Q. Mao, A. C. T. van Duin and K. H. Luo, *Carbon*, 2017, **121**, 380–388.
20 X. Mercier, O. Carrivain, C. Irimiea, A. Faccinetto and E. Therssen, *Phys. Chem. Chem. Phys.*, 2019, **21**, 8282–8294.
21 J. M. C. Marques, J. L. Llanio-Trujillo, M. Albertï¿½, A. Aguilar and F. Pirani, *J. Chem. Phys. A*, 2012, **116**, 4947–4956.
22 S. Grimme, *The Journal of Chemical Physics*, 2003, **118**, 9095–9102.
23 R. A. Kendall, T. H. Dunning, Jr. and R. J. Harrison, *J. Chem. Phys.*, 1992, **96**, 6796–6806.

24 F. Weigend and R. Ahlrichs, *Phys. Chem. Chem. Phys.*, 2005, **7**, 3297–3305.

25 O. Vahtras, J. Almöf and M. Feyereisen, *Chem. Phys. Lett.*, 1993, **213**, 514–518.

26 F. Boys and F. Bernardi, *Mol. Phys.*, 1970, **19**, 553.

27 H.-J. Werner, P. J. Knowles, R. Lindh, F. R. Manby, M. Schütz, P. Celani, T. Korona, G. Rauhut, R. D. Amos, A. Bernhardsson, A. Berning, D. L. Cooper, M. J. O. Deegan, A. J. Dobbyn, F. Eckert, C. Hampel, G. Hetzer, A. W. Lloyd, S. J. McNicholas, W. Meyer, M. E. Mura, A. Nicklass, P. Palmieri, R. Pitzer, U. Schumann, H. Stoll, A. J. Stone, R. Tarroni and T. Thorsteinsson, *MOLPRO, Version2012.1, A PACKAGE of Ab Initio PROGRAMS*, 2012, seehttp://www.molpro.net.

28 J. P. Perdew, K. Burke and M. Ernzerhof, *Phys. Rev. Lett.*, 1996, **77**, 3865–3868.

29 S. Grimme, S. Ehrlich and L. Goerigk, *J. Comput. Chem.*, 2011, **32**, 1456–1465.

30 GAUSSIAN09 Revision E.01, M. J. Frisch, G. W. Trucks, H. B. Schlegel, G. E. SCUSERIA, M. A. Robb, J. R. CHEESEMAN, G. SCALMANI, V. BARONE, B. Mennucci, G. A. Petersson, H. NAKATSUJI, M. CARICATO, X. Li, H. P. HRATCHIAN, A. F. IZMAYLOV, J. Bloino, G. Zheng, J. L. Sonnenberg, M. HADA, M. EHARA, K. TOYOTA, R. FUKUDA, J. HASEGAWA, M. ISHIDA, T. NAKAJIMA, Y. HONDA, O. KITAO, H. NAKAI, T. Vreven, J. A. Montgomery, Jr., J. E. PERALTA, F. OGLIARO, M. BEARPARK, J. J. Heyd, E. Brothers, K. N. Kudin, V. N. STAROVEROV, R. KOBAYASHI, J. NORMAND, K. RAGHAVACHARI, A. Rendell, J. C. BURANT, S. S. IYENGAR, J. TOMASI, M. Cossi, N. REGA, J. M. MILLAM, M. Klene, J. E. Knox, J. B. Cross, V. BAKKEN, C. ADAMO, J. JARAMILLO, R. Gomperts, R. E. STRATMANN, O. YAZYEV, A. J. Austin, R. CAMMI, C. Pomelli, J. W. Ochterski, R. L. MARtin, K. MOROKUMA, V. G. ZAKRZEWSKI, G. A. Voth, P. SALVADOR, J. J. DANNENBERG, S. DAPPRICH, A. D. DANIELS, O. FARKAS, J. B. FORESMAN, J. V. Ortiz, J. Cioslowski, D. J. Fox, GAUSSIAN, Inc., WALLINGford CT, 2009.

31 F. Pirani, M. Albertï¿½, A. Castro, M. M. Teixidor and D. Cappelletti, *Chem. Phys. Lett.*, 2004, **394**, 37–44.

32 N. Faginas-Lago, F. Huarte-Larraï¿½aga and M. Albertï¿½, *Eur. Phys. J. D*, 2009, **55**, 75–85.

33 F. Pirani, S. Brizi, L. F. Roncaratti, P. Casavecchia, D. Cappelletti and F. Vecchiocattivi, *Phys. Chem. Chem. Phys.*, 2008, **10**, 5489–5503.

34 M. Albertï¿½, A. Castro, A. Laganï¿½, M. Moix, F. Pirani, D. Cappelletti and G. Liuti, *J. Phys. Chem. A*, 2005, **109**, 2906–2911.

35 M. Albertï¿½, A. Aguilar, J. M. Lucas and F. Pirani, *J. Phys. Chem. A*, 2010, **114**, 11964–11970.

36 J. Nocedal, *MATH. Comp.*, 1980, **35**, 773–782.

37 D. Liu and J. Nocedal, *MATH. PROGRAM. B*, 1989, **45**, 503–528.

38 J. L. Llanio-Trujillo, J. M. C. Marques and F. B. Pereira, *Comput. Theor. Chem.*, 2013, **1021**, 124–134.

39 J. M. C. Marques, J. L. Llanio-Trujillo, M. Albertï¿½, A. Aguilar and F. Pirani, *J. Chem. Phys. A*, 2013, **117**, 8043–8053.

40 K. Deb and H.-G. Beyer, *Evol. Comput.*, 2001, **9**, 197–221.

41 F. B. Pereira, J. M. C. Marques, T. Leitï¿½o and J. Tavares, Advances in Metaheuristics for Hard Optimization, Springer Natural Computing Series, Berlin, 2008, pp. 223–250.

42 M. Bartolomei, F. Pirani and J. M. C. Marques, *J. Comput. Chem.*, 2015, **36**, 2291–2301.

43 K. Bowal, J. W. Martin, A. J. Misquitta and M. Kraft, *Combust. Sci. Technol.*, 2019, 1–19, in press; doi: 10.1080/00102202.2019.1565496.

44 H. Yuan, W. Kong, F. Liu and D. Chen, *Chem. Eng. Sci.*, 2019, **195**, 748–757.

45 S.-H. Chung and A. Violi, *Proc. Combust. Inst.*, 2011, **33**, 693–700.

46 B. S. Haynes, H. Jander and H. G. Wagner, *Symposium (INTERNATIONAL) on Combustion*, 1979, **17**, 1365 – 1374.

47 J. Simonsson, N.-E. Olofsson, H. Bladh, M. Sanati and P.-E. Bengtsson, *Proc. Combust. Inst.*, 2017, **36**, 853–860.

Table 1 Cor-K^+ and Cor-Cs^+ analytical potential parameters: well depth[a] (ε), equilibrium distance (r_0), β and m of the ILJ potential for the atom-atom pair interactions; partial charges on carbon (q_{C_i}) and hydrogen (q_H) atoms are as those reported in Ref. 10: in the case of carbons two identical charges are placed above and below the atoms and separated by 1.8 Å: q_{C_1} is the charge associated to the six inner carbon atoms, q_{C_2} that to the six intermediate carbon atoms and q_{C_3} that to the twelve outer ones.

ILJ interaction	ε / meV	r_0/ Å	β	m
C-K^+	58.290	3.300	7.5	4
H-K^+	37.628	2.827	6.0	4
C-Cs^+	48.072	3.645	8.0	4
H-Cs^+	22.529	3.328	6.0	4

partial charges / a.u.	q_{C_1}	q_{C_2}	q_{C_3}	q_H
	0.000878	-0.006000	-0.042321	0.089765

	q_{K^+}	q_{Cs^+}
	0.600	0.600

[a] 1 meV= 0.0964853 kJ mol^{-1}

Table 2 Binding energies (in kJ mol^{-1}) of the K^+Cor_n (n = 1 5) clusters obtained with both the analytical potential and after re-optimization at the DFT/PBE-D3(BJ)/cc-pVTZ level of theory.

n	analytical PES	DFT
1	-110.18	-103.03
2	-245.08	-214.26
3	-354.66	-316.27
4	-455.75	-414.38
5	-556.71	-507.14

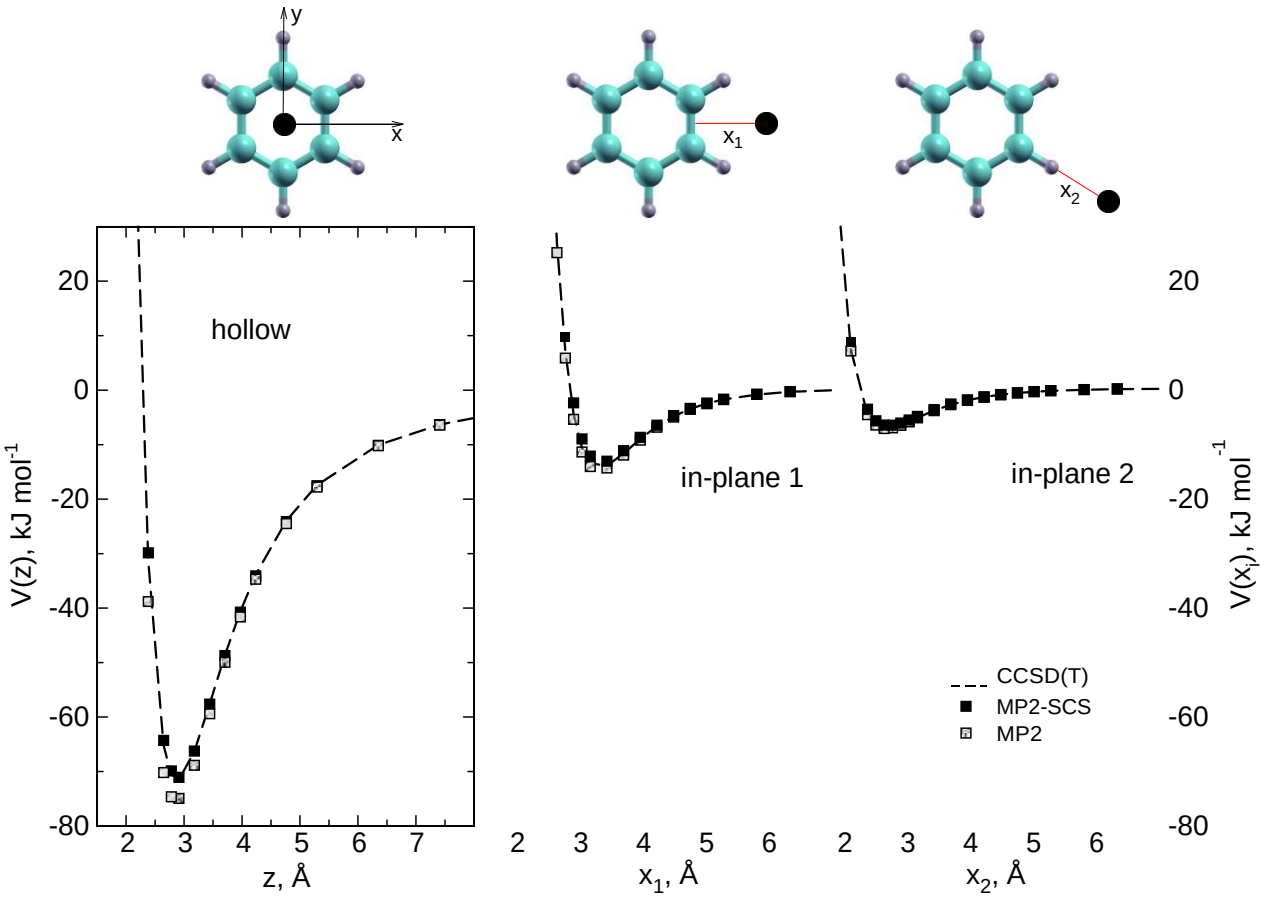

Fig. 1 Interaction energy along three different approaches of K^+ towards the benzene molecule. The first panel ("hollow") corresponds to the cation perpendicularly approaching the molecular center. The last two panels ("in-plane 1" and "in-plane 2") correspond to in-plane approaches along the x_1 and x_2 coordinates (see upper part). MP2 and MP2-SCS results are reported as shaded as full squares, respectively, while the reference CCSD(T) profiles as dashed lines.

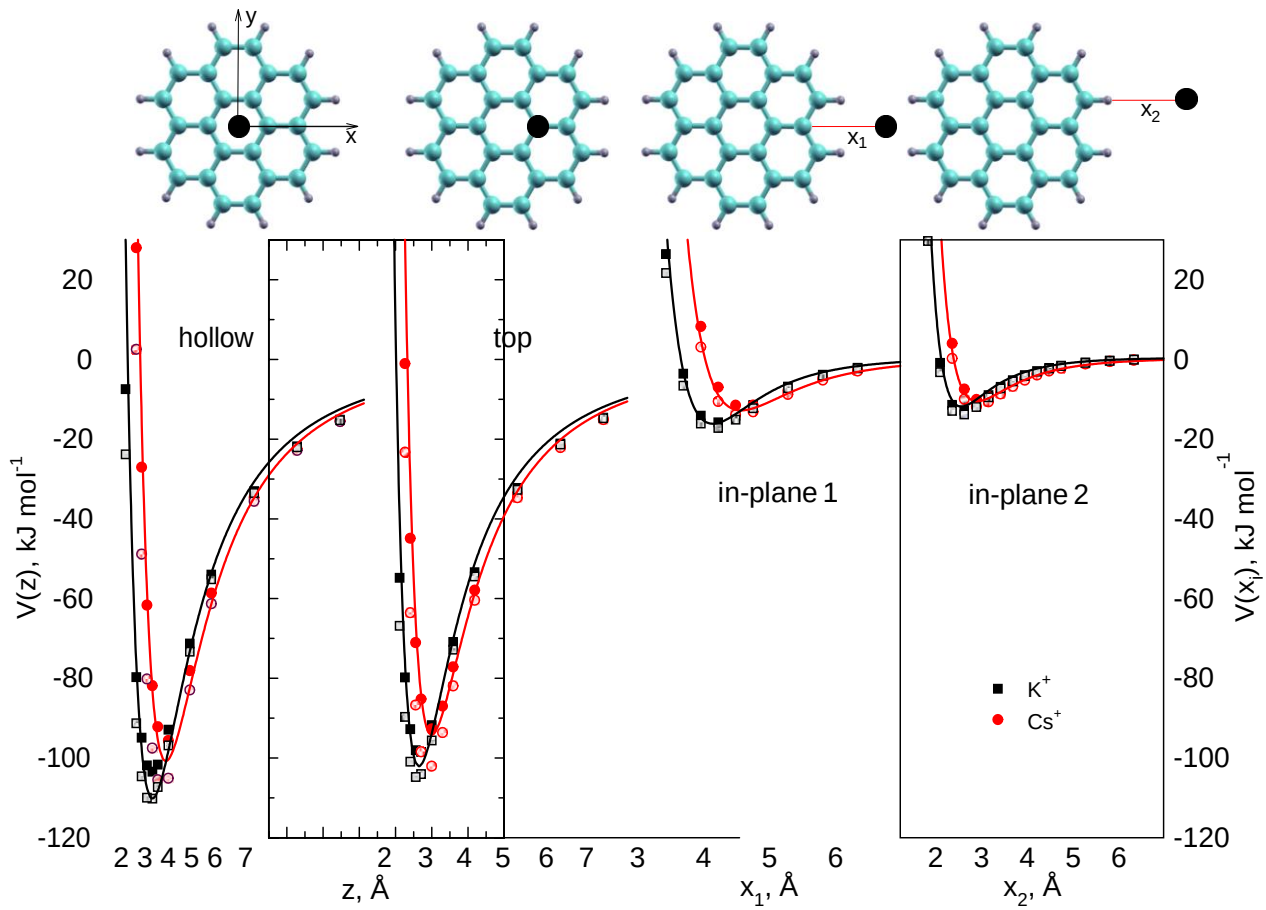

Fig. 2 Interaction energy along four different approaches of either K^+ or Cs^+ towards the coronene molecule. The first two panels ("hollow" and "top") correspond to perpendicular approaches of the cation towards the molecular center and on top of an inner carbon, respectively. The last two panels ("in-plane 1" and "in-plane 2") correspond to in-plane approaches along the x_1 and x_2 coordinates (see upper part). Squares and circles represent first-principles interaction energies (MP2 and MP2-SCS results are reported as shaded and full symbols, respectively) while solid lines correspond to the present analytic model.

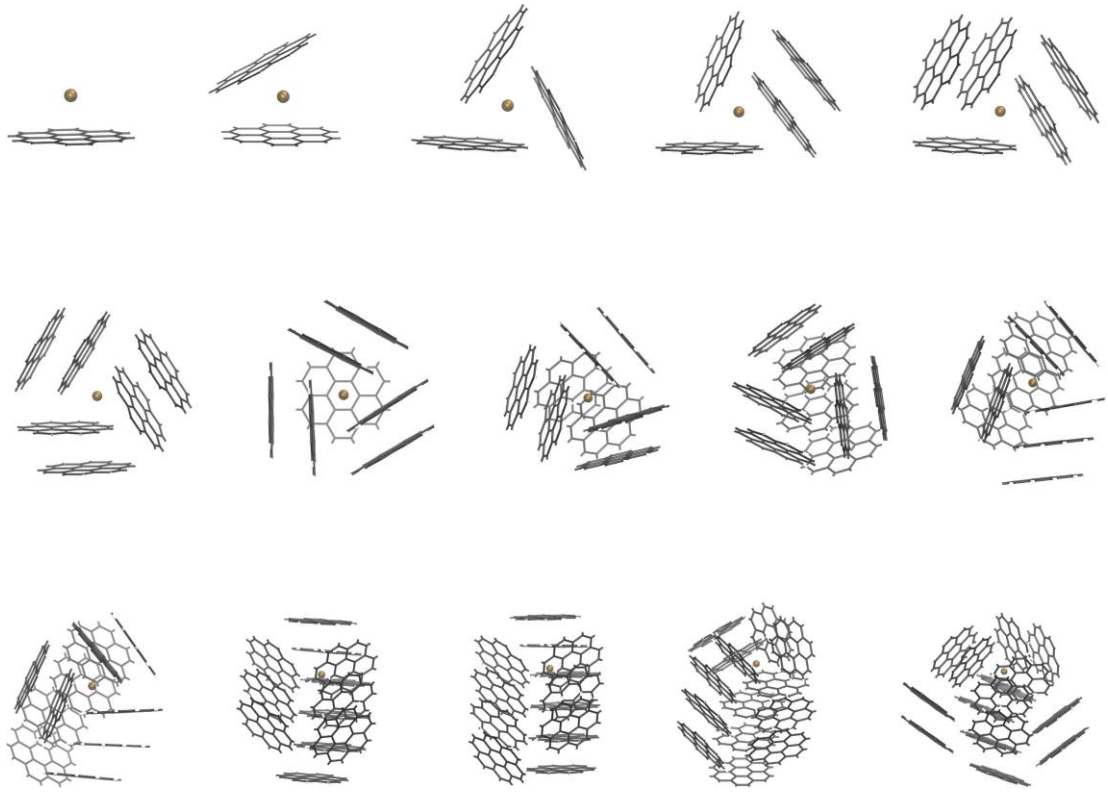

Fig. 3 Putative global minimum structures of the $K^{+}Cor_{n}$ clusters (with

$n = 1 - 15$).

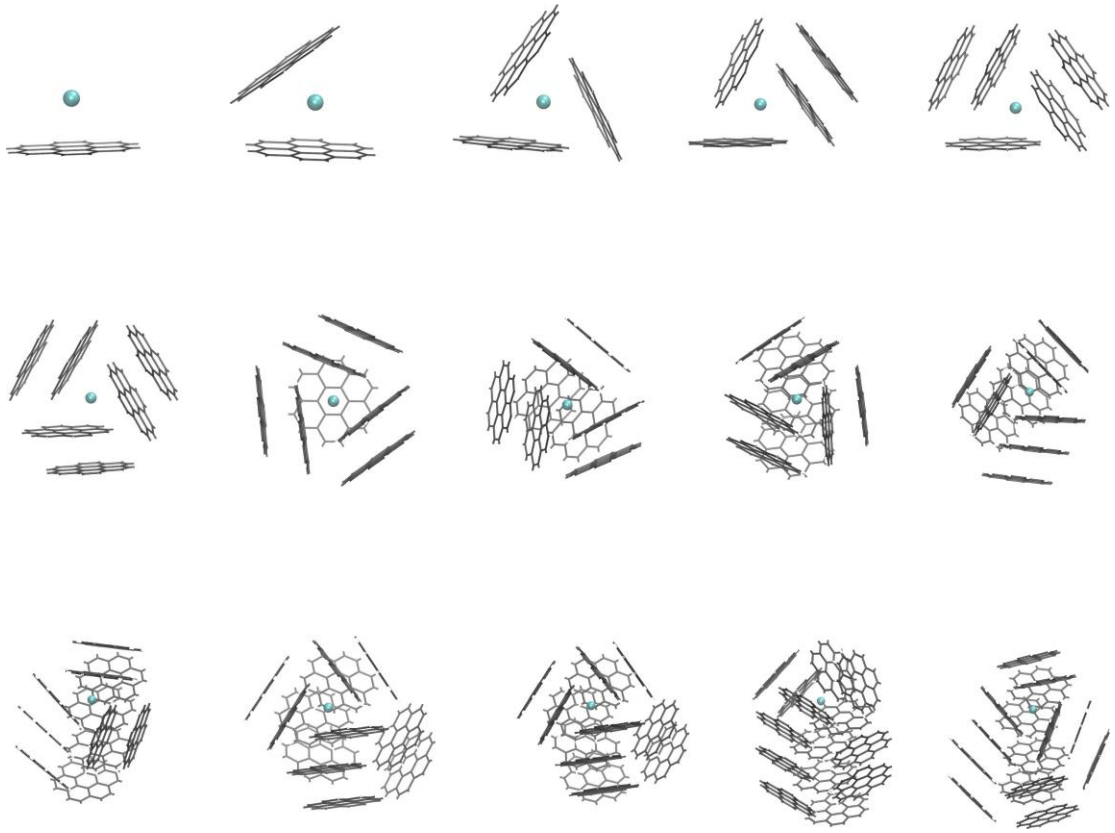

Fig. 4 Putative global minimum structures of the $Cs^{+}Cor_{n}$ clusters (with $n = 1 - 15$).

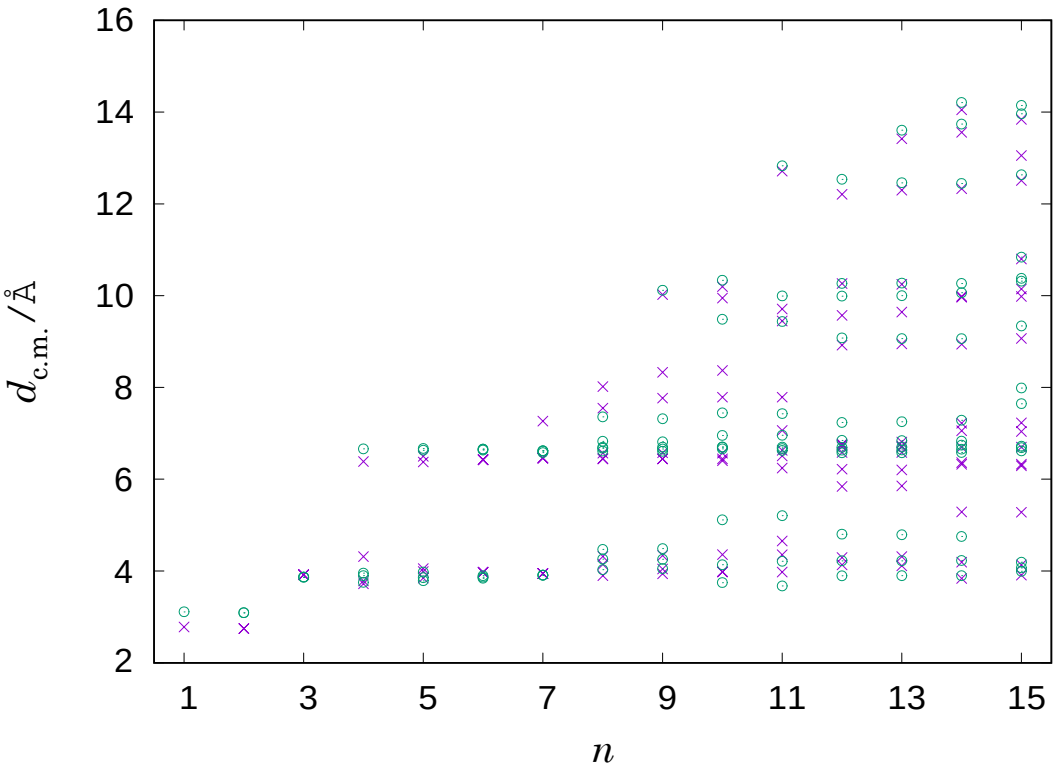

Fig. 5 Scatter plot of the distances between the alkali-ion and the center of the coronene molecules as a function of n: crosses (circles) are for K^+Cor_n (Cs^+Cor_n) clusters.

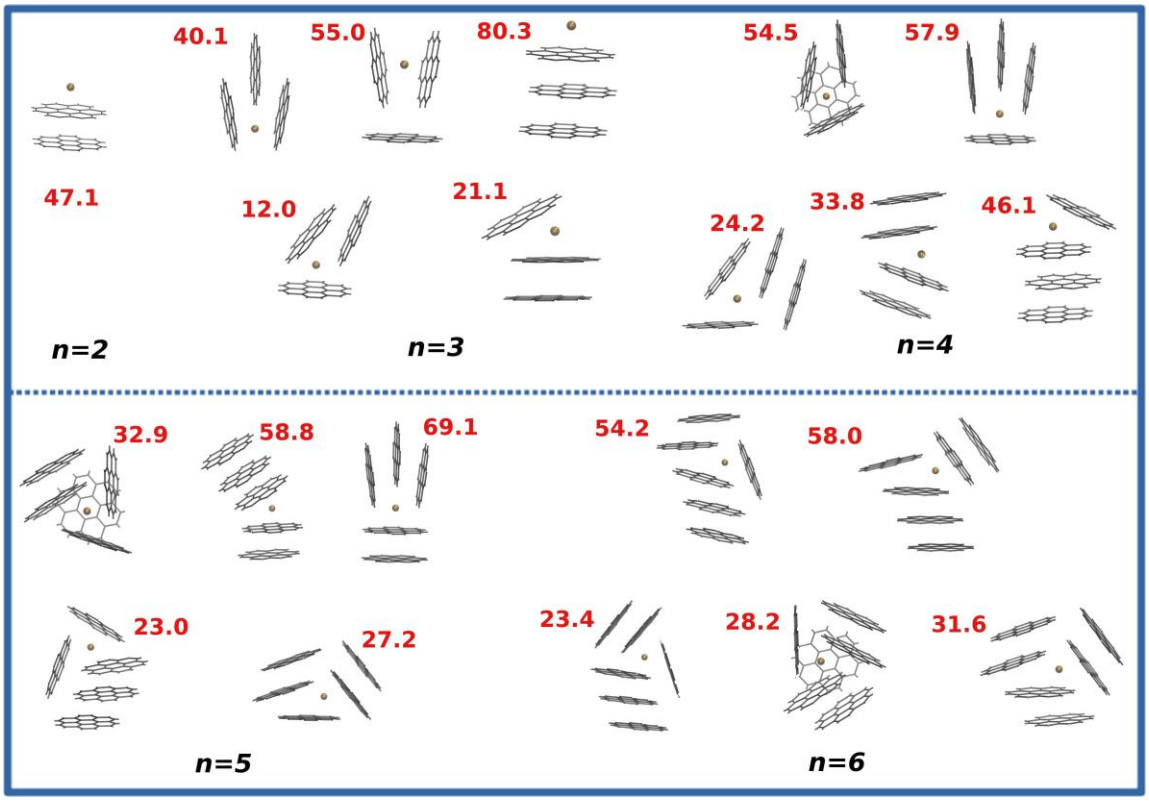

Fig. 6 Main structural motifs, other than the global minimum for the smaller K^+Cor_n clusters (with $n = 2 - 6$). For each structure, the related energy gap (in kJmol^{-1}) with respect to the corresponding global minimum is indicated by the numbers in red.

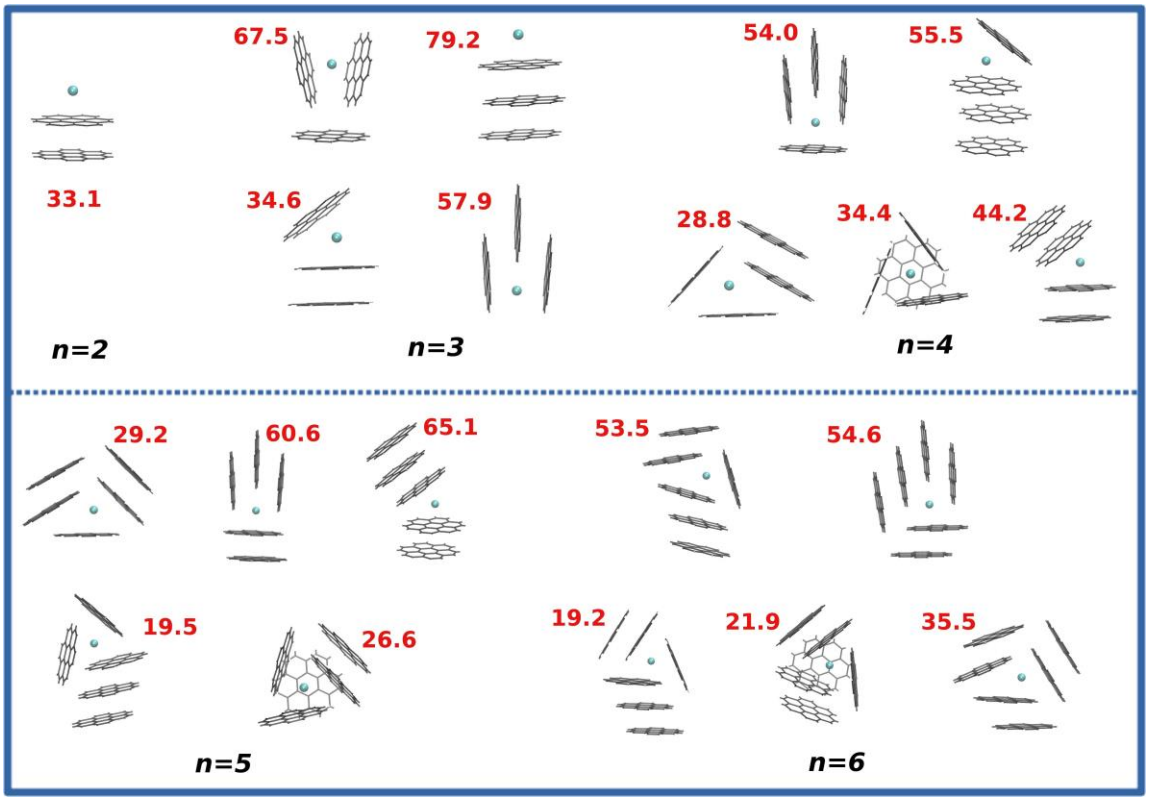

Fig. 7 As in Fig. 6, but for the $Cs^{+}Cor_{n}$ clusters (with $n = 2 - 6$).

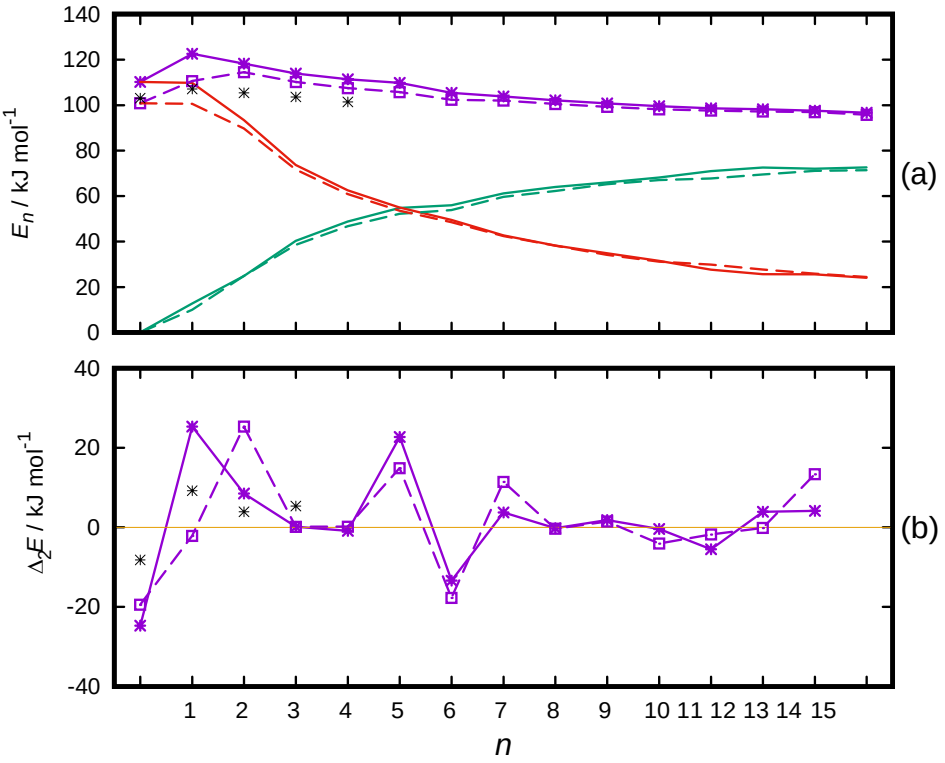

Fig. 8 Average binding energy [panel (a)] and second energy difference [panel (b)] for K^+Cor_n (solid lines) and Cs^+Cor_n (dotted lines) clusters. In panel (a), red lines denote the ion-coronene contribution for the average binding energy, while the green lines are for the coronene-coronene energy. The black asterisks in both panels represent the corresponding the DFT/PBE-D3(BJ)/cc-pVTZ values for the K^+Cor_n clusters (with $n = 1 - 5$ or $n = 1 - 4$).